INTERNATIONAL JOURNAL OF ROBOTICS
(THEORY AND APPLICATIONS)
E-mail: IJR@kntu.ac.ir

Dynamic Load Carrying Capacity of Mobile-Base Flexible-link Manipulators: Feedback Linearization Control Approach

M. H. Korayem[a], S. Firouzy[b]

a&b- Robotic Research Laboratory, Center of Excellence in Experimental Solid Mechanics and Dynamics, School of Mechanical Engineering, Iran University of Science and Technology, Tehran, Iran

ARTICLE INFO

Keywords:
Flexible Links, Mobile Base, Dynamic Load Carrying Capacity.

ABSTRACT

This paper focuses on the effects of closed- control on the calculation of the dynamic load carrying capacity (DLCC) for mobile-base flexible-link manipulators. In previously proposed methods in the literature of DLCC calculation in flexible robots, an open-loop control scheme is assumed, whereas in reality, robot control is achieved via closed loop approaches which could render the calculated DLCC value inaccurate. The aim of this research is to investigate the necessity of considering the effect of closed loop control in the calculation of the DLCC of mobile-based flexible link manipulators. Finite elements modeling and the Lagrange method have been used for modeling a mobile-base manipulator with two flexible links link. After that, a control scheme based on the feedback linearization method has been devised. A method for calculating the DLCC from a previously published study has then been utilized, with the difference that closed-loop motion control has been assumed as opposed to open-loop control. Finally, three simulation case studies have been presented for which the results have been compared with those reported in a previously published study which ignores the closed-loop control effects. The comparisons show that the effect of closed-loop control on the DLCC needs to be taken into account.

1- Introduction

This study addresses consideration of closed-loop control effects on the calculation the dynamic load carrying capacity (DLCC) of mobile-base flexible-link manipulators, using finite elements and Lagrange modeling and feedback linearization control approach. Mobile robot manipulators have increasingly been given attention during recent years due to their several advantages over their rigid counterparts; such as their improved maneuverability and their reduced power consumption. However, application of these types of robots involves dealing with a number of problems. Since mobile robots are usually “power-on-board” with limited power capacity, using light links and small actuators in order to reduce power consumption is desirable in designing these types of manipulators. As small actuators produce less torque than their heavier ones, the maximum load that can be carried by the manipulator will be constrained to a limit determined partially by the maximum available joint torques constraint. On the other hand, the flexibility of the links causes the end-effectors actual path to deviate from the desired path, and the amount of deviation at each point of the path depends on the amount of the load carried by the manipulator. Hence there are two constraints that must be taken into consideration in

finding DLCC of such manipulators, namely the actuators torque constraint, and the accuracy constraint.

Several studies could be found in the literature about finding the DLCC of different types of manipulators. Calculating the DLCC has applications in the design stage of robots; for instance, in one study Thomas et al. [1] used the load carrying capacity as a criterion for choosing the actuators of robot manipulators. Wang and Ravani [2] addressed the problem of finding the DLCC of rigid robots for a prescribed trajectory by formulating the joint actuator constraint; they introduced the concept of load coefficient. Korayem and Basu [3, 4, 5] presented an algorithm for computing the DLCC of elastic manipulators. Yue et al. [6] considered the problem of computing the maximum payload of kinematically redundant manipulators by using finite-element modeling. Korayem and Ghariblu [7] presented an algorithm for finding the DLCC of rigid mobile manipulators. Korayem and Davarpanah [8] dealt with the problem of finding the DLCC of flexible-joint manipulators with feedback linearization control. The dynamic models of flexible-joint manipulators consist of equations that are much simpler than those of flexible-link manipulators. The problem of finding the DLCC of mobile-base flexible-link manipulators has been addressed by Korayem and Heidari [9] by using finite-elements and Lagrange dynamics modeling and with open loop control (i.e. using inverse dynamics equations). They presented an algorithm for finding the DLCC and presented simulation results of a case study of a planar flexible two-link manipulator mounted on a mobile base.

Several studies on motion control of flexible arm robots could be found in this literature. Some of them have considered design of regulator-type controllers where the robot arm end-point is to be located in a desired position rather than to track a desired trajectory [10]. Rattan and Feliu applied feed-forward control to a flexible link robot and reported simulation results of the system step response, with the joint angle as the controlled output [11]. Geniele et al. [12] considered tip position control for regulating purposes. They used a linear controller and presented simulation results of the system step response.

Several researches have focused on joint angle trajectory tracking of flexible link robot manipulators [13-15]. Yan, et al. [16] applied partial feedback linearization for tracking control of joint angles of a single flexible link robot. Loukinove et al. [17], proposed joint angle trajectory tracking control during the motion with an alternative control loop to suppress vibrations at the end of the motion. Wai and Lee [18] applied intelligent optimal control for joint angle tracking of a flexible link robot. The problem of controlling flexible-link manipulators poses different challenges to the designer of control strategy due to the vibratory nature of such systems; such systems have passive degrees-of–freedom and are therefore categorized among under-actuated systems, therefore full state feedback linearization can not be applied to them. Instead, partial feedback linearization method could be utilized for such systems, aiming to control joint angles while keeping the internal dynamics (i.e. vibrations of the links) stable. Although some research could be found in the literature that has addressed the problem of controlling the end effecter position of flexible link manipulators on a set point (i.e. regulator type controller design), in trajectory tracking motion control (i.e. servo control) the conventional control strategy is join angles control (rather than arm tip position control) which has also been used in the current research.

Neither one of the studies in the literature have taken into consideration the effects closed loop control on calculating the DLCC of mobile-base flexible-link manipulators. Although a similar task has been done in [7] for flexible-joint manipulators, applying this approach for flexible-link manipulators brings about new problems that will be revealed in the simulation stage. This is because the highly nonlinear dynamic equation of these types of robots makes it hard to implement closed loop control. Furthermore, finding the DLCC without considering the effect of closed-loop control, as done in [6] and [9], has one major defect: robots used in industrial applications operate with closed-loop rather than open-loop control algorithms. Therefore the presence of a controller could alter the actual value of DLCC calculated with the assumption of open-loop case, as will be demonstrated in this article.

In this paper a flexible two-links planar manipulator mounted on a mobile base has been presented, and a model based on finite element modeling and Lagrange dynamics has been used. Next, a control strategy using a feedback linearization technique has been set up for motion control of the manipulator on a given end-effector trajectory. A criterion for finding the dynamic load carrying capacity of the manipulator has then been presented, which is based on a previously published work [9], with the only difference that closed loop control has been assumed. After that, through computer simulation, the application of the presented method has been shown for a case study of a planar flexible two link manipulator mounted on a mobile base. Finally, two additional case studies have been presented with simulation parameter identical to those reported in [9] wherein DLCC was calculated assuming open-loop

control, and a comparison has been made in order to evaluate the effect of feed-back linearization control on the value of DLCC.

2- Modelling of the flexible manipulator

2-1- Model development

Consider a planar two-link manipulator with links 1 and 2 as depicted in Fig.1. This planar manipulator is in the horizontal plane and therefore the gravity vector is perpendicular to the plane of Fig.1. The model used here is two-dimensional, i.e. only deflection of the links in the plane of motion of the manipulators has been considered. Therefore, gravity has no effect on the deflection of the links of the robot model used here, and the deflections are caused only by the motion of the robot arms. The mobile base can move in the plane along x and y, and the distance of the base from the origin of the fixed coordinate system is shown with x_0 and y_0. Consider link 1 to be divided into elements '11','12',…,'1j',…'1 n_1' of lengths all equal to l_1, and link 2 to be divided into elements '21','22',…,'2j',…'2 n_2' of lengths all equal l_2, (Fig. 1). n_1 and n_2 are the numbers of the elements of links 1 and 2, respectively. In the simulation study presented in this paper, one element is used for each link for simplicity, therefore n_1 and n_2 are both equal to 1. Let us define the following notations (where subscript i refers to link i, and subscript ij refers to the jth element of link i): OXY is the fixed system of coordinates, $O_iX_iO_iY_i$ is the body-fixed coordinate system attached to link i. O_1X_1 is the direction of the inflexed link 1. O_2X_2 is the direction of the inflexed link 2. u_{2j-1} is the flexural displacement at the common junction of the two elements '1(j-1)' and '1j' of link 1. u_{2j} is the flexural slope at the tip of common junction of elements '1(j-1)' and '1j' of link 1. This slope is measured with respect to axis O_1X_1. w_{2j-1} is the flexural displacement at the common junction of elements '2(j-1)' and '2j' of link 2, and w_{2j} is the flexural slope at the common junction of elements '2(j-1)'and '2j' of link 2. This slope is measured with respect to axis O_2X_2. θ_1 and θ_2 are the rotation angles of the first and the second joints, respectively.

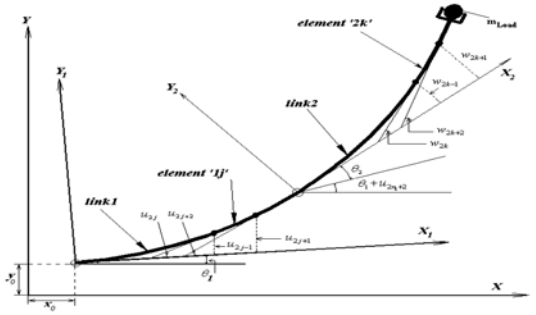

Fig. 1: Schematic of the flexible link robot

The model development approach is described in detail in [9], and the final form of the equations of the model is as follows:

$$\mathbf{M}\,\ddot{\mathbf{q}} - \mathbf{f} = \mathbf{Q} \qquad (1)$$

Where $\mathbf{M} = \mathbf{M}(\mathbf{q})$ is a 7×7 matrix and $\mathbf{f} = \mathbf{f}(\mathbf{q}, \dot{\mathbf{q}})$ is a column vector of nonlinear functions of the generalized coordinates vector $\mathbf{q}$, and its rate of change $\dot{\mathbf{q}}$. In this case, after applying boundary conditions, some of the generalized coordinates associated with link deflections will be constantly equal to zero, so that the generalized coordinates vector will be: $\mathbf{q} = [x_0 \quad \theta_1 \quad u_3 \quad u_4 \quad \theta_2 \quad w_3 \quad w_4]^T$. The first row of the vector Q in eq. (1) denotes the force $\mathcal{F}$ applied to the base of the manipulator along its path, and the second and fifth rows contain the values of torques applied at joints, namely τ_1 and τ_2, and rest of the rows are zeros; i.e., $\mathbf{Q} = [\mathcal{F} \quad \tau_1 \quad 0 \quad 0 \quad \tau_2 \quad 0 \quad 0]^T$. The differential equation of the position of the end-effector is:

$$\ddot{\mathbf{P}} = \mathbf{J}\ddot{\mathbf{q}} + \dot{\mathbf{J}}\dot{\mathbf{q}} \qquad (2)$$

Where $\mathbf{P}$, $\dot{\mathbf{P}}$ and $\ddot{\mathbf{P}}$ are the vector of the position of the end-effector and its time derivatives respectively, and $\mathbf{J}$ and $\dot{\mathbf{J}}$ are the Jacobian matrix and its time derivative respectively.

2-2-Model adjustment for control-law deriving

In order to utilize the model of the manipulator in deriving the control law, the model has to be changed into a more convenient form. Consider eq. (1), in which seven scalar differential equations are assembled into a matrix equation. The first scalar equation mentioned in the first row of the matrix eq. (1) describes the behavior of the manipulator base position x_0. In this study we only aim to control the tip position trajectory and we assume that the manipulator base is forced to follow a predefined

path. The value of x_0 is thus a function of time and the first row of the matrix equation must be eliminated. By omitting the first row of all matrices in (1), the differential equation of the system will become:

$$\mathbf{M}'\ddot{\mathbf{q}} - \mathbf{f}' = \mathbf{Q}' \quad (3)$$

where $\mathbf{M}'$ and $\mathbf{f}'$ are obtained by eliminating the first rows of $\mathbf{M}$ and $\mathbf{f}$, and $\mathbf{Q}' = [\tau_1 \quad 0 \quad 0 \quad \tau_2 \quad 0 \quad 0]^T$. Now, those terms of the equations containing $\ddot{x}_0$ (the second time-derivative of x_0) must be brought to the right side of the equation because $\ddot{x}_0$ will be replaced by a predefined function of time. Since $\ddot{x}_0$ is on the first row of $\ddot{\mathbf{q}}$, the first column of $\mathbf{M}'$ is multiplied by $\ddot{x}_0$ in eq. (3). We therefore separate the first column of $\mathbf{M}'$, name it $\mathbf{M}''_1$, and multiply it by $\ddot{x}_0$. Then, eq. (3) changes into the following form:

$$\mathbf{M}''_2\ddot{\mathbf{q}}' + \mathbf{M}''_1\ddot{x}_0 - \mathbf{f}' = \mathbf{Q}' \quad (4)$$

Where $\mathbf{q}' = [\theta_1 \quad u_3 \quad u_4 \quad \theta_2 \quad w_3 \quad w_4]^T$, and $\mathbf{M}''_2$ is obtained by eliminating the first column of $\mathbf{M}'$. By multiplying both sides of the equation by $(\mathbf{M}''_2)^{-1}$ and defining $\mathbf{F} = (M''_2)^{-1}(f' - M''_1\ddot{x}_0)$, eq. (4) becomes:

$$\ddot{\mathbf{q}}' = \mathbf{F} + (\mathbf{M}''_2)^{-1}\mathbf{Q}' \quad (5)$$

Since there are four zero rows in $\mathbf{Q}'$, four of the columns of $(\mathbf{M}''_2)^{-1}$ are multiplied by zeros in eq. (5); therefore by eliminating them, the equation describing the behavior of the generalized coordinates of the whole system will become:

$$\ddot{\mathbf{q}}' = \mathbf{F} + \mathbf{G}\boldsymbol{\tau} \quad (6)$$

Where $\boldsymbol{\tau} = [\tau_1 \quad \tau_2]$ and $\mathbf{G}$ is a 6×2 matrix obtained by eliminating the four zero-columns of $(\mathbf{M}''_2)^{-1}$ (namely the second, third, fifth and sixth columns).

The system has six generalized coordinates, two of which correspond to the joint angles, namely θ_1 and θ_2, and the other four variables denote deflections of the links, namely u_3, u_4, w_3 and w_4. For control law computation purposes, it is appropriate to separate these two groups of variables and their differential equations. Therefore, by selecting the first and fourth rows of (6), the differential equation of the joint angles could be represented separately as:

$$\ddot{\boldsymbol{\theta}} = \mathbf{F}_\theta + \mathbf{G}_\theta\boldsymbol{\tau} \quad (7)$$

Where $\boldsymbol{\theta} = [\theta_1 \quad \theta_2]^T$, while $\mathbf{F}_\theta$ and $\mathbf{G}_\theta$ are 2×2 square matrices comprised only of the first and fourth rows of $\mathbf{G}$ and $\mathbf{F}$, respectively. The differential equation of the rest of the generalized coordinates could be represented in a matrix form as follows:

$$\ddot{\mathbf{q}}_f = \mathbf{F}_f + \mathbf{G}_f\boldsymbol{\tau} \quad (8)$$

Where the subscript 'f' refers to the flexural variables of the system and $\mathbf{q}_f = [u_3 \quad u_4 \quad w_3 \quad w_4]^T$. $(\mathbf{F}_f)_{4\times1}$ and $(\mathbf{G}_f)_{4\times2}$ are obtained by omitting the first and fourth rows of $\mathbf{G}$ and $\mathbf{F}$, respectively.

3-Joint-Angle Trajectory Tracking Control

3-1-Control Scheme

The feedback linearization control method has been utilized in this study to address the problem of end-effector motion control of flexible link manipulators, which are categorized amongst under-actuated systems and therefore full state feedback linearization cannot be applied to them. Instead, partial feedback linearization (or input-output feedback linearization) is used to control joint angles. The problem of stability of the internal dynamics of the system (which, in this case, correspond to the vibrations of the links) has been addressed in section 3-2 and stability has been checked after simulation of the manipulator motion along the desired path. Simulations have been conducted via Simulink toolbox of Matlab software.

The control scheme is based on deriving the desired joint angles trajectory from the desired end-effector trajectory (inverse kinematics). The joint angles are calculated in a fashion in which they would correspond to the end-effector desired path, neglecting links deflection. This means that, assuming link rigidity, tracking the obtained trajectory for join angles would result in tracking the desired end-effector trajectory; obviously, this is not the case here because the deflections of the links will cause the end effector position to deviate from its desired position at each point of the path. The amount of this deviation, which must not exceed the allowable limits, depends on the amount of the load carried by the end-effector and is one of the two criteria by which the DLCC is calculated. Considering eq. (7), the following control law leads to asymptotic tracking of the desired joint angles trajectory:

$$\boldsymbol{\tau} = \mathbf{G}_{\theta}{}^{-1}[-\mathbf{F}_{\theta} + \boldsymbol{\nu}] \quad (9)$$

Where $\boldsymbol{\theta}_{\mathrm{d}} = [\theta_{1\mathrm{d}}\ \theta_{2\mathrm{d}}]^{\mathrm{T}}$ is the desired joint angle vector as a function of time, $\tilde{\boldsymbol{\theta}} = \boldsymbol{\theta} - \boldsymbol{\theta}_{\mathrm{d}}$ is the tracking error vector and $\boldsymbol{\nu}$ is the new input of the system defined by:

$$\boldsymbol{\nu} = \ddot{\boldsymbol{\theta}}_{\mathrm{d}} - \lambda_1 \dot{\tilde{\boldsymbol{\theta}}} - \lambda_2 \tilde{\boldsymbol{\theta}} \quad (10)$$

The torques calculated in (9) should be applied to the manipulator, as demonstrated in the block diagram in Fig. 2. Applying the control law of eq. (10) leads to a linear relationship between the system outputs and the new input $\boldsymbol{\nu}$, i.e. $\ddot{\boldsymbol{\theta}} = \boldsymbol{\nu}$. It could be seen by comparing eq. (7), (9) and (10) that the above-mentioned control law will cause the dynamic equation of the joint angles to become:

$$\ddot{\tilde{\boldsymbol{\theta}}} + \lambda_1 \dot{\tilde{\boldsymbol{\theta}}} + \lambda_2 \tilde{\boldsymbol{\theta}} = \mathbf{0} \quad (11)$$

This is a linear differential equation in which proper choice of λ_1 and λ_2 will lead to the asymptotic convergence of the tracking error to zero. This is a problem of placing the poles of the linearized closed-loop system, which must be located on the left hand side of the vertical axis in the complex number plane. Here, the optimum locations of the closed loop poles were chosen by trial and error, and the corresponding values of λ_1 and λ_2 are 1.1 and 0.1, respectively.

3-2-Stability of the Closed-Loop System

The stability problem of flexible-link manipulators with joint-motion control has been addressed in published researches [13, 20, and 22]. Feedback linearization control, with the choice of joint angles as the controlled output of the system, has been shown to be efficient in maintaining stability. In order to explain the stability analysis, let us consider the system dynamic equations (7) and (8) again. Eq. (7) describes the input-output behavior of the system, while it does not show another part of the system dynamics (namely the internal dynamics), which is described in eq. (8). The control law of eq. (9) causes the behavior of the system output to follow the linear differential equation of (10), provided that the internal dynamics are stable; otherwise the control approach is impractical since the internal instability (i.e. boundlessly increasing vibrations of the links) will render the entire system unstable. The internal dynamics of the system is coupled with the observable output dynamics of the system and internal stability analysis can be carried out by studying the so-called *zero dynamics* of the system. Zero dynamics equations of the system are obtained by constraining the output θ of the system to be kept constantly equal to zero using appropriate inputs. It has been shown in [21] that the stability of the zero dynamics together with the use of a control law like that of eq. (9) will lead to stability of the entire system in regulating control (where the control objective is to keep the output constantly zero), provided that the linear equation of the output (eq. 11) is stable (i.e. the constants λ_1 and λ_2 are chosen so that the roots of the characteristic equation are on the left hand side of the vertical axis in the complex number plane). It has also been shown that in joint-motion tracking control of flexible link manipulators, the zero dynamics are stable [20].

In the case of tracking control (where the outputs are supposed to follow a desired path), the analysis is slightly different as follows. Keeping in mind that the internal dynamics described by eq. (8) is dependent on the behavior of the input-output dynamics of eq. (7), we need to convert the internal dynamics in eq. (8) into a form in which the input $\boldsymbol{\tau}$ is not explicitly mentioned [21]. Therefore, by substituting eq. (9) into eq. (8), the following equation of internal dynamics during the joint-angle motion control is obtained:

$$\ddot{\mathbf{q}}_{\mathrm{f}} = \mathbf{F}_{\mathrm{f}} + \mathbf{G}_{\mathrm{f}}(\mathbf{G}_{\theta}{}^{-1}[-\mathbf{F}_{\theta} + \ddot{\boldsymbol{\theta}}_{\mathrm{d}} - \lambda_1 \dot{\tilde{\boldsymbol{\theta}}} - \lambda_2 \tilde{\boldsymbol{\theta}}]) \quad (12)$$

Provided that the answer of eq. (12) exists, is limited and is stable, the whole system is stable and the control law of (9) will lead to asymptotic tracking of the desired outputs [21]. Furthermore, as long as all time varying functions of the internal dynamics of eq. (12) are bounded (which is the case in the numerical examples used in this paper), stability is ensured, even during trajectory tracking [20]. Diagrams of the flexural variables of the system during output trajectory tracking have been included in this paper in order to confirm the stability of the internal dynamics and to assure that the link vibrations have remained bounded throughout the motion.

It should be noted that although the abovementioned stability analysis does not explicitly involve the Cartesian coordinates of the end-effector position, it still implies the stability of the end-effector position. This could be seen by considering that the values of the end-effector coordinates are determined by the joint angles as well as the flexural variables (i.e. u_3, u_4, W_3 and W_4). On the other hand, stability of the internal dynamics means that the flexural variables remain limited and stable. Therefore, while the joint angles trace their desired values and as long as the internal dynamics are stable, the end-effector position coordinates also remain limited and stable.

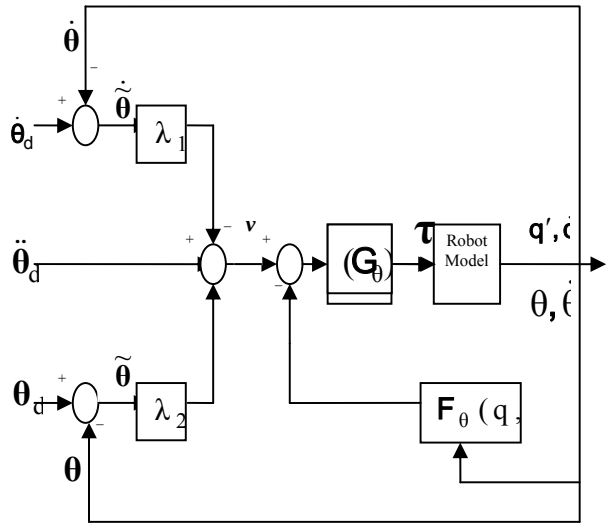

Fig. 2: Block diagram of the control scheme. Note that joint angles vector (θ) is controlled.

4- Formulation of the Dynamic Load Carrying Capacity (DLCC) for a Predefined Trajectory

The DLCC calculation method presented here is similar to the one proposed in [9]. The only difference is that between the DLCC formulation in this study and the one reported in [9] is that the closed loop control has been taken into consideration in the current study.

The DLCC of a flexible link mobile manipulator for a given trajectory is defined as the maximum load that the manipulator can carry along the desired trajectory with acceptable precision. In the case of flexible-link manipulators, link flexibilities can cause deviation of the end-effector trajectory from its desired one. Therefore, a constraint on the end-effector deflection must be imposed, as well as one on the motor torques.

4-1- Formulation of the accuracy constraint

As illustrated in [9], the method for formulating the accuracy constraint is based on discretising the trajectory into separate points. Performing simulations, no-load deflection $(\mathrm{Def_n})_j$ and deflection with added end effector mass $(\mathrm{Def_e})_j$ are computed for each point of the digitized trajectory. As depicted in Fig. 3, both the magnitude and the direction of the deflection change by adding the end-effector mass. But as long as the magnitude of the deflection is not greater than the maximum allowable value, the robot is considered to remain capable of executing the given trajectory. Therefore only the magnitude of the deflection needs to be considered. Hence, a series of spherical boundaries with radii equal to R_p (maximum allowable deviation) and centered at points on the digitized desired trajectory have been introduced, as shown in Fig. 3. Although the no-load deflection ($\mathrm{Def_{nl}}$) and the deflection due to the end effector load ($\mathrm{Def_e}$) are generally vectors of different directions, the increase of the deflection magnitude due to the added mass at the end effector is linearly related to the mass [5 and 19].

The difference between the magnitudes of the allowable deflection and the deflection due to the added end-effector mass will be:

$$R_p - (\mathrm{Def_e})_j \tag{11}$$

This can be regarded as the remaining allowable end-effector deflection at point j of the given trajectory. This remaining amount can express the amount of additional load that can be carried along the desired trajectory without violating the maximum allowable deviation of the end-effector position. Therefore, a load coefficient $(C_p)_j$ can be introduced for point j of the discritised trajectory, j=1,2,…,m as :

$$(C_p)_j = \frac{R_p - (\mathrm{Def_e})_j}{\max[\mathrm{Def_e}] - \max[\mathrm{Def_{nl}}]} \tag{12}$$

Where

$$\max\{\mathrm{Def_e}\} = \max\{(\mathrm{Def_e})_1, (\mathrm{Def_e})_2, ..., (\mathrm{Def_e})_m\}$$
$$\max\{\mathrm{Def_{nl}}\} = \max\{(\mathrm{Def_{nl}})_1, (\mathrm{Def_{nl}})_2, ..., (\mathrm{Def_{nl}})_m\} \tag{13}$$

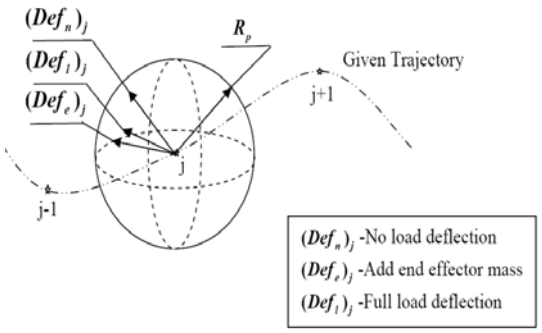

Fig. 3: Spherical boundary of the end effector deflection

4-2. Formulation of the actuator torque constraint

The formulation of the actuator torque constraint for rigid manipulators could be found in [8]. The same approach could be used for flexible manipulators as well, as in [6]. In order to formulize the actuator torque constraint, knowledge of the maximum allowable torques of the motors is needed; therefore, typical torque-speed curves of DC motors

have been used [5] here. Considering $k_1 = T_s$ and $k_2 = T_s/\omega_{nl}$ where T_s is the stall torque and ω_{nl} is the maximum no-load speed of the motor, the upper and lower bounds of the allowable motor torques, U^+ and U^-, could be found using the following relation:

$$U^+ = k_1 - k_2\dot{q}$$
$$U^- = -k_1 - k_2\dot{q} \quad (14)$$

Similar to the process of calculating the accuracy constraint, here we need to run the simulation twice; once without any load (also excluding the end effector) and once with the end effector load, as described in [8]. By performing computer simulation, the torque at joint i for the no-load case (τ_{nl}) and the torque due to the end effector load (τ_e) are calculated according to the control law for the motion of the manipulator which can be obtained for each point of the discretised trajectory. Note that for the case that the end effector load has been taken into account, the total torque applied is equal to $\tau_{nl} + \tau_e$. The available torque for carrying the load will be:

$$\tau_i^+ = (U^+)_i - (\tau_e)_i - (\tau_{nl})_i$$
$$\tau_i^- = (U^-)_i - (\tau_e)_i - (\tau_{nl})_i \quad (15)$$

and the maximum allowable torque at the ith joint will be equal to:

$$(\tau_a)_i = \max\{\tau_i^+, \tau_i^-\} \quad (16)$$

Now a load coefficient could be defined to represent the actuator torque constraint, as follows:

$$(C_a)_j = \min\{(\tau_a/\tau_e)_i \quad , i = 1,2,...,n\} \quad (17)$$

Where the subscript 'i' denotes the i'th joint, and "n" is the number of the joints. The load coefficient $(C_a)_j$, from a physical point of view, describes the accessible load for carrying the maximum load divided by the load applied for carrying the initial load. Finally, the load coefficient C can be obtained as follows:

$$C = \min\{(C_p)_j, (C_a)_j\} \qquad j = 1,2,...,m \quad (18)$$

where "m" is the number of the points of the discretised trajectory. The maximum load m_{load} that can be carried on the trajectory without violating either of the two constraints will be:

$$m_{load} = C \times m_e \quad (19)$$

where m_e is the mass of the end effector.

5-Simulation Results and Discussion

The simulation results for three case studies of flexible-link mobile-base manipulators are presented here. The first case study is presented for a thorough description of the approach, and all of the necessary diagrams have been shown. The second and third case studies are presented in order to compare the results with a previously published work [9], and therefore only the diagrams that were necessary for the purpose of comparison have been shown for those two cases.

5-1- First Case Study: A Complete Demonstration of the Procedure

The characteristics of the manipulator used in the simulation of the first case study are presented in Table 1.

TABLE 1. Parameters Used in the First Simulation

Parameter	Value	Unit
Length of the links	$L_1 = L_2 = 1.2$	m
Moment of Inertia	$I_1 = I_2 = 5.5e-8$	m^4
Mass per Length	$m_1 = m_2 = 0.8$	*Kg/m*
Modulus of Elasticity	$E_1 = E_2 = 2.0e11$	N/m^2
k_1	160	$N.m.$
k_2	10	$N.m.s/ra$

Simulations were performed two times, first for the manipulator without load and then for an initial load of 0.5 kg. The maximum allowable deflection of the end-effector was considered to be 0.03 m. The results of the simulation of the manipulator motion with the initial load have been depicted in Fig. 4 to 10. Fig. 4 shows the desired and the actual path of the end-effector with the initial load. In Fig. 5 and 6 show the first and the second actuator torques with their upper and lower limits. Figs. 7 to 10 show that the flexural variables of the system have been kept limited to small values, which confirms the internal stability of the closed loop system. The base of the manipulator travels on the OX axis as in Fig. 1, and its distance from the origin O is defined by:

$$x_0(t) = 0.0937t^5 - 0.4687t^4 + 0.625t^3$$

The desired path of the end-effector was chosen to be:

$$\mathbf{y}_d(t) = \begin{bmatrix} x_0(t) + 1.84 \\ 0.15 + 0.15\mathrm{Sin}(4\pi t - \pi/2) \end{bmatrix}$$

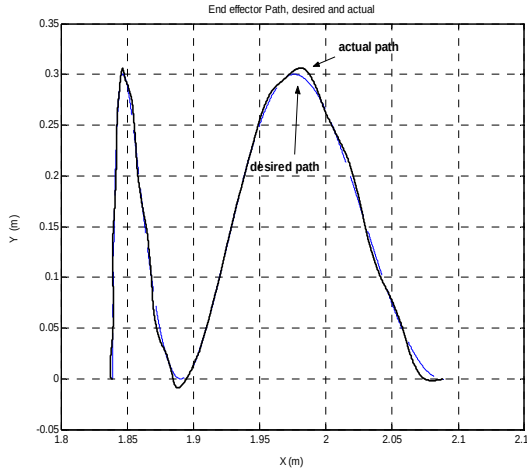

Fig. 4: Desired and actual path of the end effector with initial load

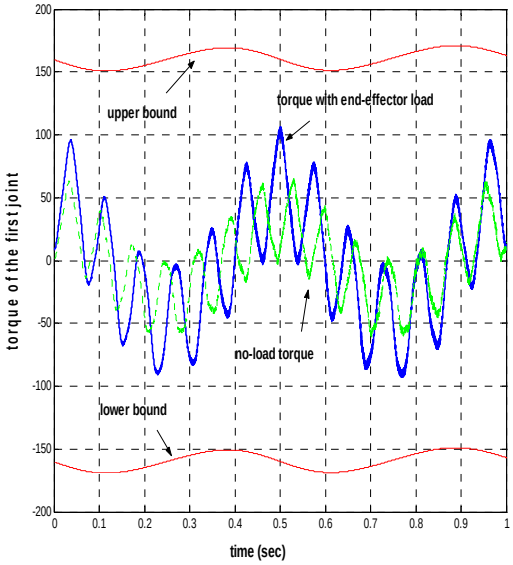

Fig. 5: Torque of the first joint actuator, without load and with the initial load, and its upper and lower boundaries

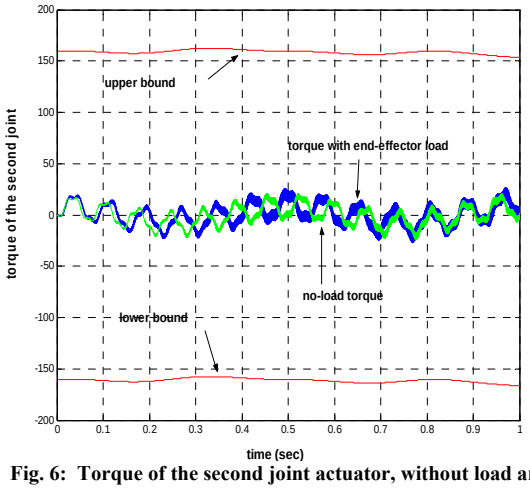

Fig. 6: Torque of the second joint actuator, without load and with the initial load, and its upper and lower boundaries

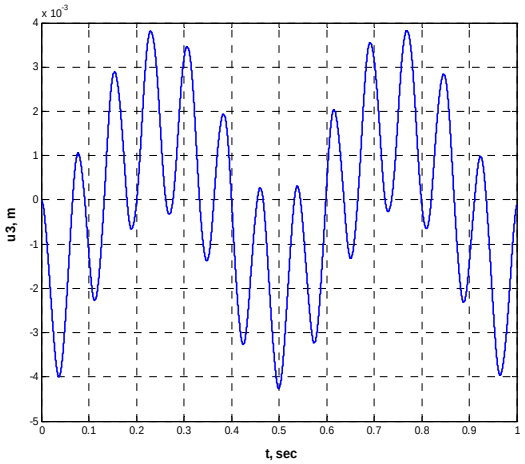

Fig. 7: Deflection of the tip point of the first link, u_3

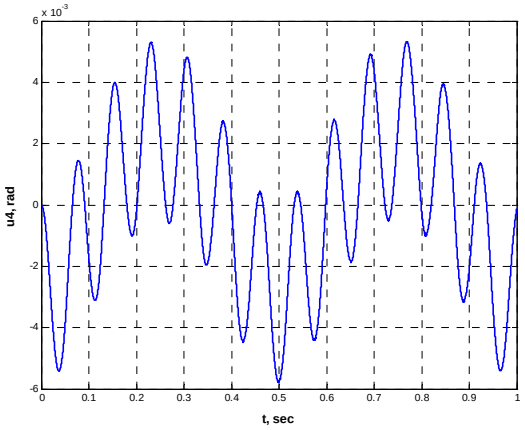

Fig. 8: Flexural slop at the tip point of the first link, u_4

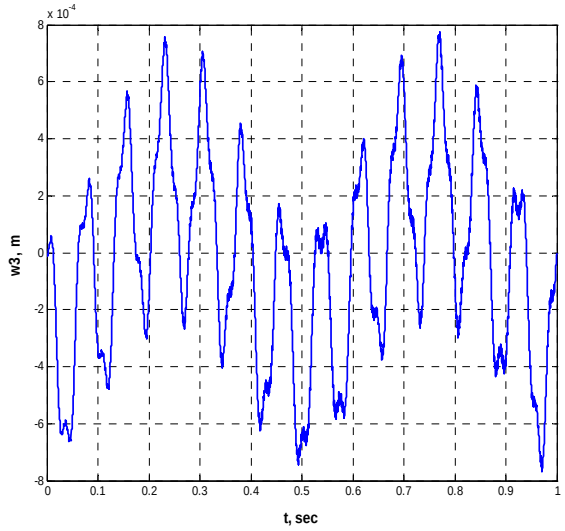

Fig. 9: Deflection of the tip point of the second link, w_3

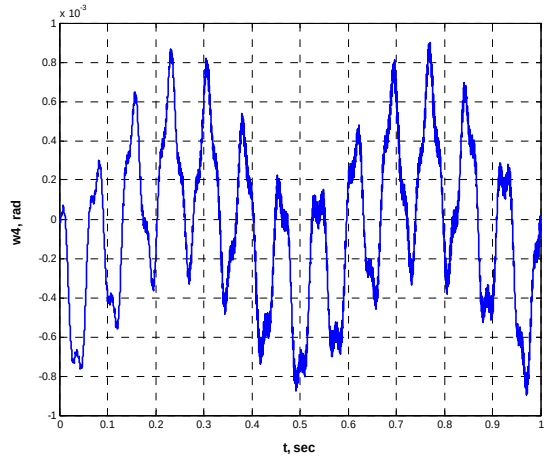

Fig. 10: Flexural slop at the tip point of the second link, w_4

The DLCC of the manipulator calculated by equation (19) was found to be 1.37 kg. Two constraints, namely the accuracy and the motor torques constraints were considered for finding the DLCC, which in this case the motor torques constraint was the dominating constraint; i.e., the manipulator would be capable of carrying a heavier load without violating the accuracy constraint if the motors could produce more torque. In order to verify the reliability of the DLCC calculation method, a test was performed in which the motion of the manipulator with the computed maximum load was simulated. It was expected that the manipulator would be able to carry the load without violating the accuracy constraint and that at least one of the motors torques would reach its maximum available bound, since the motor torque constraint determined the DLCC. This could be seen in Fig.11 to 13. Fig.11 shows the desired and the actual path of the end effector while carrying the maximum load. Fig.12 shows the deviation of the end effector from the desired path throughout the motion of the manipulator, which is clearly far from exceeding the maximum allowable value (0.03 m). Fig.13 shows that the first joint torque has reached its maximum allowable value near the point t=0.5 sec. The torque of the second joint is also shown in Fig.14; a comparison between Fig.13 and 14 shows that the saturation of the first joint actuator (rather than the second one) torque is the dominant constraint which determines the maximum load that the manipulator can carry.

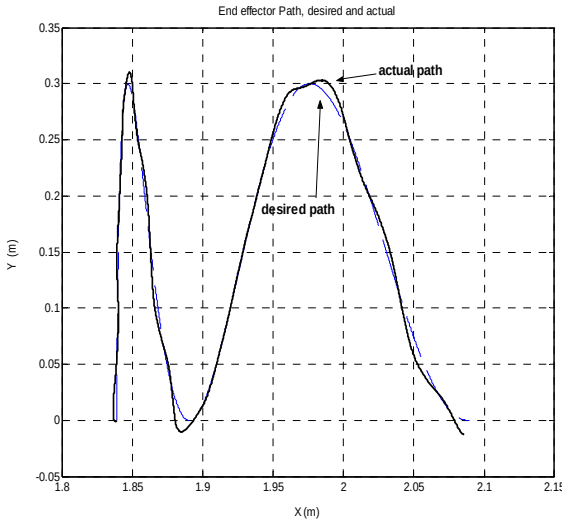

Fig.11: Desired and actual path of the end effector with maximum load

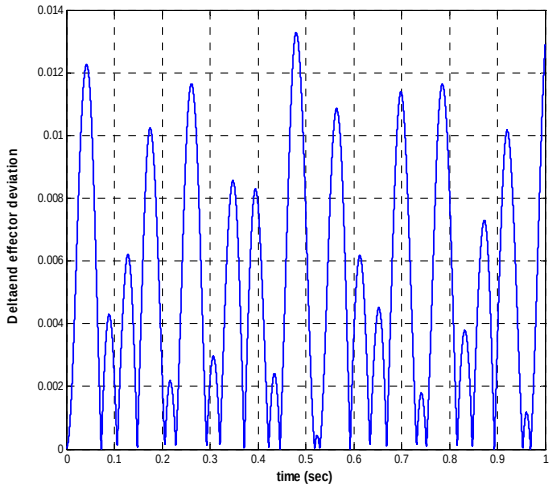

Fig.12: deviation of the end effector from the desired path while carrying the maximum load

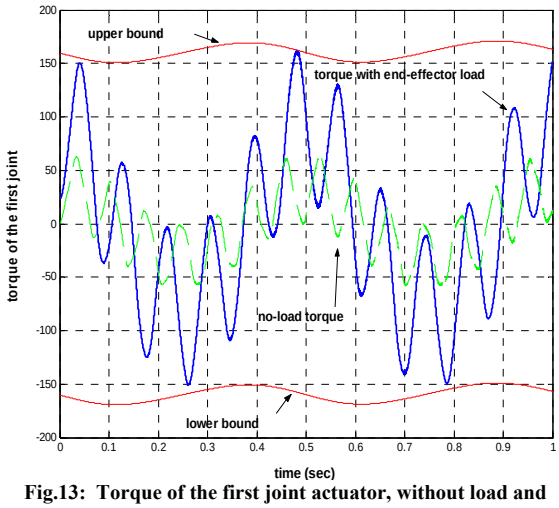

Fig.13: Torque of the first joint actuator, without load and with the maximum load, and its upper and lower boundaries

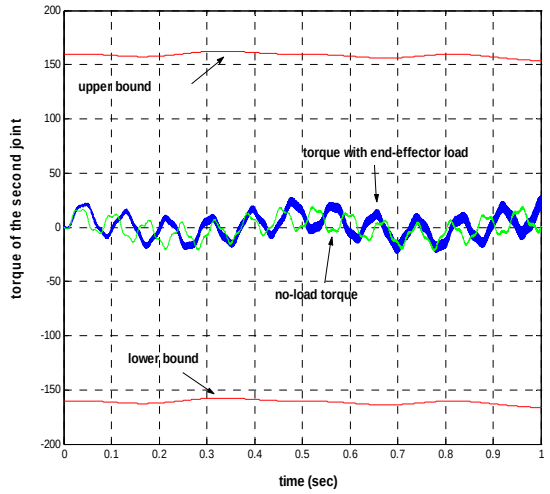

Fig.14: Torque of the second joint actuator, without load and with the maximum load, and its upper and lower boundaries

5-2- Second Case Study: Comparison with a previously published study

In the second case study, the problem parameters have been chosen to be identical to those reported in [9], in which the DLCC of a flexible-link mobile-base manipulator is calculated without assuming closed-loop control (i.e. using inverse dynamics approach). Results of the simulation have been brought here to be compared to those reported in [9] in order to see the effect of feedback linearization control on the value of the DLCC. The parameters used in the simulation are given in Table 2. The path of the end-effector and its load is a strait line, starting from point $\{x_1 = 0\,m \quad , y_1 = 2\,m\}$ and ending at point $\{x_1 = 0.76\,m \quad , y_1 = 2.38\,m\}$, as depicted in Fig.15.

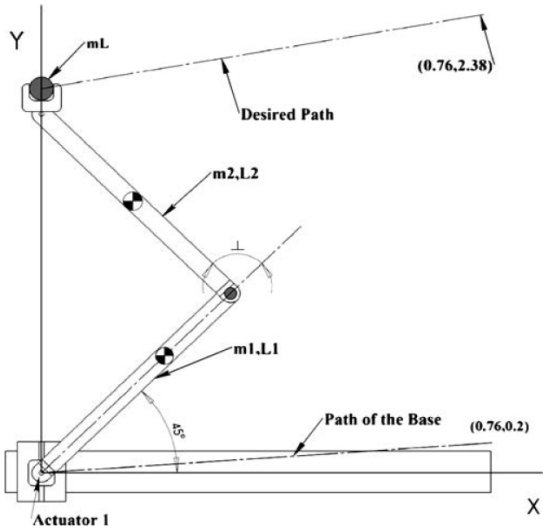

Fig.15: Schematic of the robot and the end-effector path in the second case study

The desired velocity profile of the end effector along its path is as follows:

$$\begin{cases} v = at & 0 \le t \le T/4 \\ v = v_{\max} & T/4 < t \le 3T/4 \\ v = v_{\max} - at & 3T/4 \le t \le T \end{cases}$$

where T=3.25 sec. The permissible error bound for the end-effector position around each point on the desired path is limited to R=0.03 m. A linear path is planned for the vehicle, which starts from the origin and ends at the point ($x_{b2} = 0.76\,m \quad , y_{b1} = 0.2\,m$), with the velocity of $V_b = a_b t$. The procedure of calculating the DLCC is the same as the previous case. Fig.16 shows the desired and the actual path of the end-effector. Figs.17 and 18 show the torques of the actuators with and without the initial load and Figure19 shows the diagram of DLCC for the given path against time, with a minimum of 0.25 kg.

The path of the manipulator while carrying the maximum load, (which is equal to 0.25 kg) is shown in Fig. 20. It could be seen that the accuracy bound is far from being violated in this case. Fig. 21 shows the torque of the first joint actuator, and it can be seen that at the end of the motion, the torque of the second actuator has taken its maximum allowable value.

The DLCC value calculated here shows no increase in comparison to that reported in [9] where open loop control has been assumed. This could be explained by the following analysis:

In this case study, the constraint that determines the DLCC is the actuator torques constraint rather than the accuracy constraint, in other words, the accuracy of tracking the desired end-effector position is unimportant here. On the other hand, although closed loop control increase tracking accuracy, it does not necessarily decrease the control effort (and in this case, it has not). It should also be noted that the value of the DLCC calculated here was not neither reduced compared to the open loop case. This could be explained by considering that a closed-loop control scheme does not necessarily lead to *greater* actuator torques compared to the open-loop case, but rather more *precisely calculated* torques. Therefore, in cases where actuator torque limitation is the dominating constraint, calculating the DLCC yields the same result whether or not closed loop control has been considered.

The sudden jump in the DLCC diagram in Fig.19 could be explained this way: as mentioned earlier, through most of the motion period, the actuator torques constraint is stricter than the accuracy constraint i.e. $C_a < C_p$ for most of the motion period. But approximately at $t = 0.6\,\text{sec}$, the *no-load torque* (τ_{nl}) and the *torque with end effector load* $(\tau_{nl} + \tau_e)$ at the first joint have equal values, as could be seen in Fig.17. This means that at this moment $\tau_e = 0$ for the first joint. By considering eq. (17) it is found that at this moment, C_a of the first joint approaches infinity and its value will be increasing rapidly before this moment. Thus, the load coefficient (which is defined as the minimum of C_p and C_a of the two joints) will increase at this time until the C_a of the first joint becomes greater than C_a of the second joint, or greater than C_p. After a short time, as could be seen in Fig.17, the difference between the *no-load torque* (τ_{nl}) and the *torque with end effector load* (which is equal to $\tau_{nl} + \tau_e$) at the first joint becomes noticeable, causing C_a to become small again.

TABLE 2. Parameters used in the second simulation

Parameter	Value	Unit
Length of links	$L_1 = L_2 = 1.414$	m
Moment of inertia	$I_1 = I_2 = 5.5e-4$	Kg.m2
Mass	$m_1 = 0.7, \quad m_2 = 0.5$	Kg
Spring Constant	$K_1 = 15, \quad K_2 = 10$	N.m
Actuator stall torque	$K_{s_1} = 18, \quad K_{s_2} = 25$	N.m.s/rad

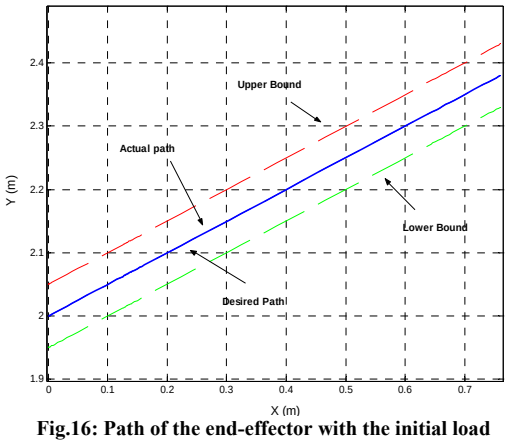

Fig.16: Path of the end-effector with the initial load

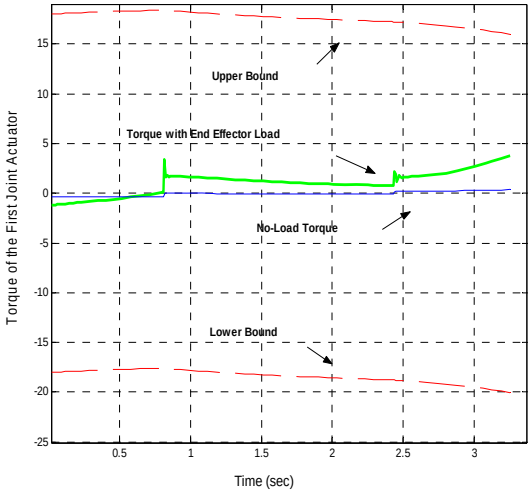

Fig.17: Torque of the first joint actuator with and without the initial load.

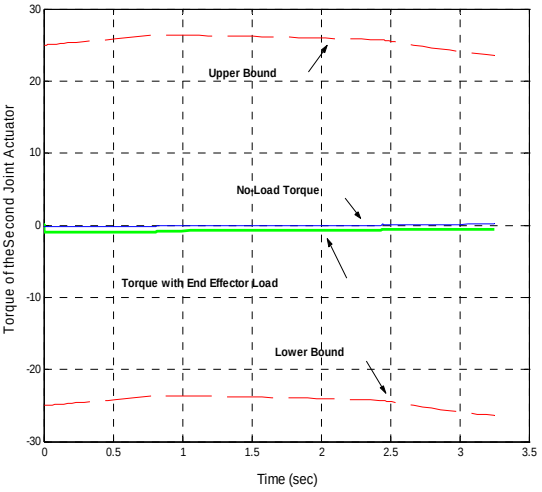

Fig.18: Torque of the second joint actuator with and without the initial load

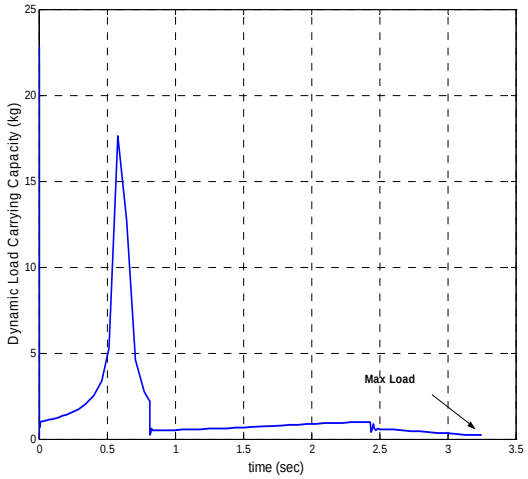

Fig.19: Dynamic Load Carrying Capacity

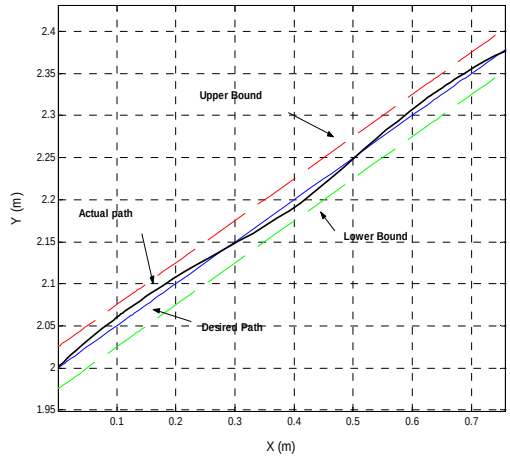

Fig. 20: Path of the end-effector with the maximum allowable load

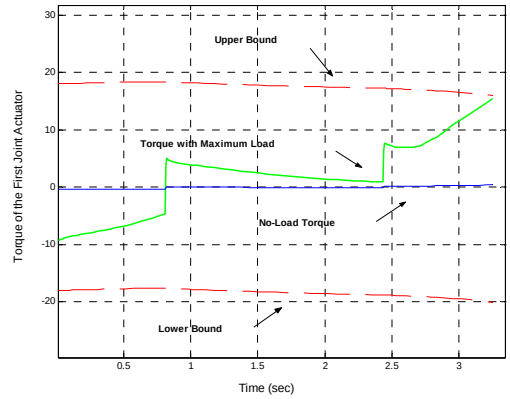

Fig. 21: Torque of the first joint actuator while carrying the maximum allowable load

5-3- Third Case Study: Comparison with a previously published study

The case study considered in [9] has been re-examined, and a comparison of the results is presented here. Schematic of the manipulator and the end-effector path is shown in Fig. 22, and the parameters used in the simulation are given in Table (3). The base moves horizontally with a velocity of $V_b = 0.5t$. The trajectory of the load is a circular path with its center located at $\{x_c = 1m, \quad y_c = 1m\}$ and a radius of $r = 50\,cm$. The motion starts from the lower point of the arc (Fig. 26) and circulates around the center of the arc in a clockwise direction. The maximum allowable error-bound at each point of the desired path is restricted to a sphere centered on the desired path with a radius of 5 cm.

TABLE. 3: Parameters Used in the Second Simulation

Parameter	Value	Unit
Length of links	$L_1 = L_2 = 1.2$	m
Moment of inertia	$I_1 = I_2 = 5.5e-4$	Kg.m2
Mass	$m_1 = 0.8, \quad m_2 = 0.8$	Kg
Spring Constant	$K_1 = 17, \quad K_2 = 12$	N.m
Actuator stall torque	$K_{S_1} = 12, \quad K_{S_2} = 30$	N.m.s/rad

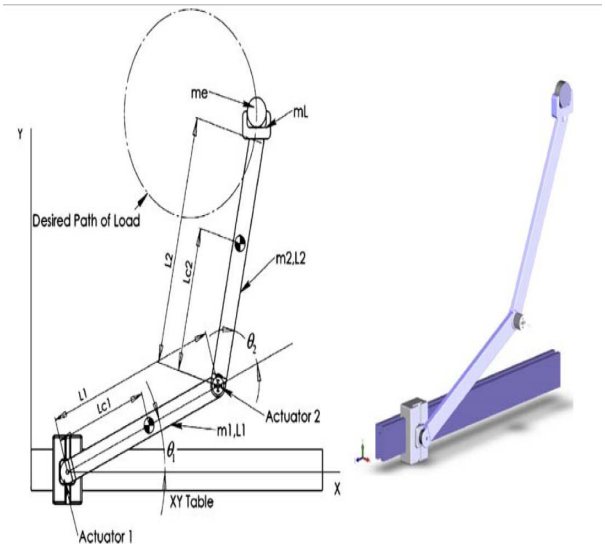

Fig. 22: Schematic view of the flexible link manipulator of the third case study

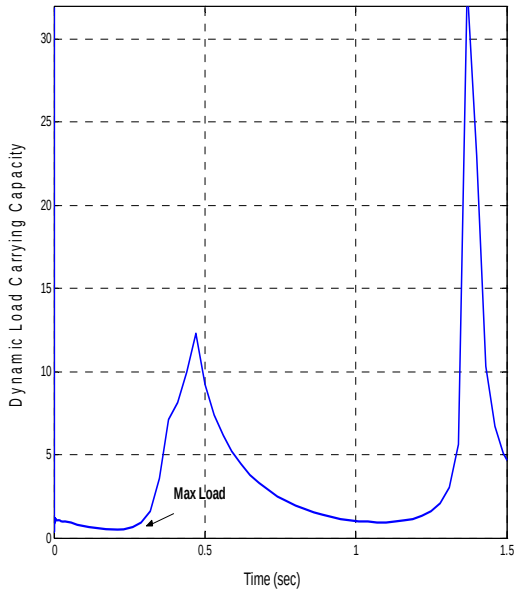

Fig. 23: Dynamic Load Carrying Capacity in the third case study

The DLCC in this case is shown in Fig. 23 with a minimum of 0.77 kg. The sudden jumps in the DLCC diagram could be explained in a similar way as in the first case study, with the difference that in this case the sudden increases in the precision load coefficient C_p (rather than the actuator torques coefficient) causes the jumps. That is, at two moments during the motion of the manipulator, namely approximately $t = 0.45\,\text{sec}$ and $t = 1.4\,\text{sec}$, the deflection of the end effector from the desired path is zero. This will cause an increase in the load coefficient C_p (the dominant coefficient in this case), as could be seen by considering eq. (12).

Joint angles are depicted in Fig. 24 and 25. The dominating constraint in this case is the accuracy constraint, as could be seen in Fig. 26 which shows that the end effector position deviation from the desired path reaches the maximum allowable value at one point during the motion. Comparison with [9] shows that the calculated DLCC has been increased by 43 percent as a result of considering closed loop control. This could be explained by considering the fact that it is the accuracy constraint that determines the DLCC in this case. Therefore, by using closed-loop control, the position of the end-effector could be controlled more precisely and therefore heavier loads (as compared to the open loop case) could be carried without violating the accuracy constraint.

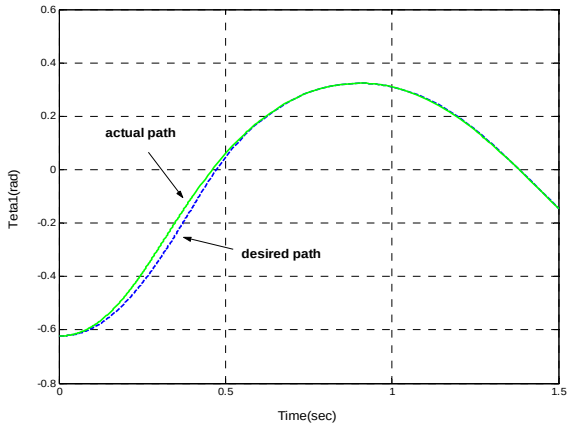

Fig. 24: Angle of the first joint during the motion of the manipulator

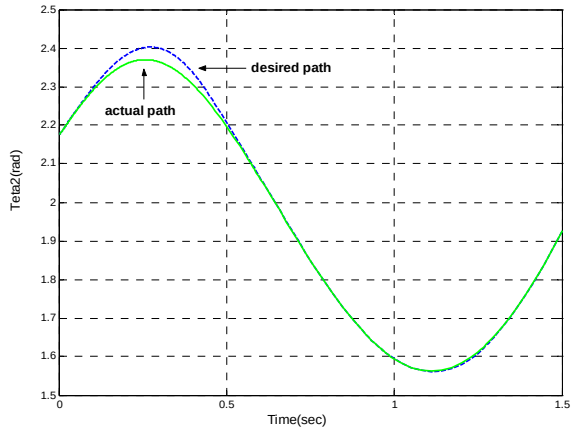

Fig. 25: Angle of the second joint during the motion of the manipul

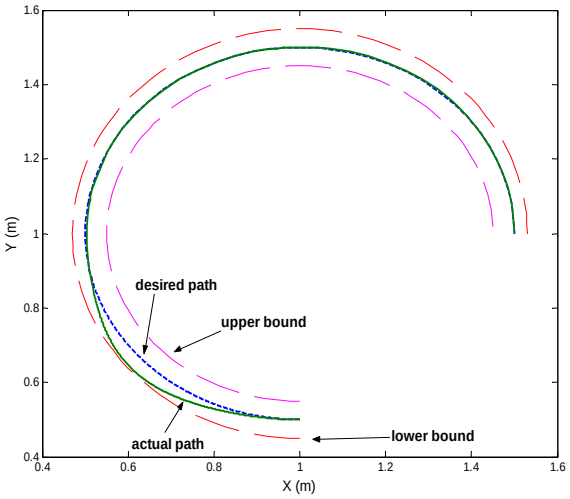

Fig. 26: Desired and actual path of the end-effector for the third case study

6- Discussion of the results and conclusion

A comparison between this case study and the second case study shows a pattern, as follows:

- In the second case study where the dominating constraint was the torque constraint, considering the effects of closed loop control did not affect the calculated value for DLCC.
- In the third case study where the dominating constraint was the accuracy constraint, it has been revealed that neglecting closed-loop control effects (i.e. improved accuracy compared to open loop case) leads to underestimation of the DLCC. Therefore, since closed-loop control is implemented in robotic applications, the DLCC calculated for the third case study here is more realistic than the one reported in [9].

The modeling and simulation process involved in DLCC calculation does not become much more complicated as a result of considering closed loop control. Therefore, in a general case, it could be concluded that closed loop control should be considered in the calculation of the DLCC of mobile-base flexible-link manipulators. On the other hand, in cases where the torque constraint is more restricting than the accuracy constraint, the DLCC value calculated with the assumption of open loop control is still reliable.

REFERENCES

[1] Thomas M, Yuan-Chou HC, Tesar D., "Optimal Actuator Sizing for Robotic Manipulators Based on Local Dynamic Criteria" J. of Mechanisms Transmission Automation in Design, Vol.107, 1985, pp. 163–169.

[2] Wang LT, Ravani B (1988) "Dynamic load carrying capacity of mechanical manipulators", Part I, problem formulation. J Dyn Syst Meas Control 110:46–52.

[3] Korayem M. H., Basu A. "Formulation and Numerical Solution of Elastic Robot Dynamic Motion with Maximum Load Carrying Capacity" Robotica, Vol.12, 1994, pp. 253–261.

[4] M. H. Korayem, A. Basu, "Mathematical Modeling and Simulation of Differentially Wheeled Mobile Robots Dynamic Equations," Int. Journal of Applied Science and Computations, Vol. 10, 2003, PP. 30-37.

[5] M. H. Korayem, A. Basu, "Dynamic load carrying capacity of robotic manipulators with joint elasticity imposing accuracy constraints", Robotics and Autonomous Systems 13 (1994) 219-229.

[6] Yue S., Tso S. K., Xu W. L., "Maximum Dynamic Payload Trajectory for Flexible Robot Manipulators with Kinematic Redundancy" Mechanism and Machine theory, Vol. 36, 2001, PP. 785-800.

[7] Korayem M. H., Ghariblu H., "Maximum Allowable Load on Wheeled Mobile Manipulators Imposing Redundancy Constraints" J. of Robotic and Autonomous Systems, Vol.44, No.2, 2003, PP. 151–159.

[8] M. H. Korayem, F. Davarpanah, H.Ghariblu, "Load carrying Capacity of Flexible-Joint Manipulators with Feedback Linearization", International Journal of Advanced Manufacturing Technology, Vol. 29, No. 3 and 4, 2006.

[9] M. H. Korayem, A. Heidari, A. Nikoobin, "Maximum Dynamic Allowable Load of Flexible Mobile Manipulators Using Finite Element Approach", International Journal of Advanced Manufacturing Technology, Vol. 36, No.5-6, 2008, PP. 606-617.

[10] Swee P. Goh, Andrew R. Plummer and Michael D. Brown," Digital Control of a Flexible Manipulator", Proceedings of the American Control Conference, Chicago, Illinois, June 2000.

[11] Kuldip S. Rattan and vincente Feliu, "Feedforward Control of Flexible Manipulators", Proceedings of the 1992 IEEE, International Conference On Robotics and Automation, Nice, France-May 1992.

[12] H. Geniele, R. V. Patel, *Fellow*, *IEEE,* and K. Khorasani, "End-point Control of a Flexible – link manipulator: theory and Experiments", IEEE Transactions on Control Systems Technology, Vol. 5, No. 6, November 1997.

[13] Alessandro De Luca, Stefano Panzieri, Giovanni Ulivi, "Stable Inversion Control for Flexible Link Manipulators", Proceedings of the IEEE, International Conference on Robotics and Automation, Leuven, Belgium, May 1998.

[14] Xu Bo, Kenji Fujimoto, Yoshikazu Hayakawa, "Control of Two Link Flexible Manipulators via Generalized Canonical Transformation", Proceedings of the 2004 IEEE, International Conference on Robotics , Automation and Mechatronics, Singapore,1-3 December, 2004.

[15] Yuchen Zhou, "Tracking Control of Multiple Flexible Link Robots", Proceedings of the 1993 IEEE/RSJ International Conference on Intelligent Robots and Systems, Yokohama, Japan July 26-30, 1993.

[16] Liu Yan, Gao Yanmei, Wang Dalong, Lu Youfang, Liu Yu, "Variable Structure Controller Design of a Two-Link Rigid-Flexible Robotic Manipulator", 1997 IEEE International Conference on Intelligent Processing Systems, October 28-31, Beijing, China.

[17] A. A. Loukianov, Y.Q. Dai, M. Uchiama, "Trajectory Tracking of Spatial Flexible Link Manipulators Using Inverse Kinematics Solution and Vibration Suppression", ICAR '97, Monterey, CA, July 7-9, 1997.

[18] Rong-Jong Wai, *Member, IEEE,* and Meng-Chang Lee, "Intelligent Optimal Control of Single-Link Flexible Robot Arm", IEEE Transactions of Industrial Electronics, Vol. 51, No, 1, February 2004.

[19] D. A. Fresonke, E. Hernandez and D. Tesar, "Deflection prediction for serial manipulators", Proc. IEEE Int. Conf. Robotics and Automation (1988) 482-487.

[20] Alessandro De Luca, Bruno Siciliano, "Inversion-Based Nonlinear Control of Robot Arms with Flexible Links", AIAA J. of Guidance, Control, and Dynamics, vol. 16, pp. 1169--1176, 1993.

[21] Jean-Jacques E. Slotine, Weiping Li, "Applied Nonlinear Control", Prentice Hall, 1991.

[22] Wang Dalong, Lu Youfang, Liu Yan,* Li Xiaoguang, "Dynamic Model and Tip Trajectory Tracking Control for a Two-Link Flexible Robotic Manipulator", IEEE International Conference on Systems, Man, and Cybernetics, 1996.

[23] Arisoy, A.; Gokasan, M.; Bogosyan, O, "Partial Feedback Linearization Control of a Single Flexible Link Robot Manipulator", proceedings of 2nd International Conference on Recent Advances in Space Technologies, 2005. RAST 2005.